

# Optical and structural properties of graphene oxide-incorporated polyvinylpyrrolidone/copper ternary nanocomposites (PVP/Cu/GO) films

A. U. Agobi<sup>a,b,c</sup>, A. I. Ikeuba<sup>c</sup>, A. J. Ekpunobi<sup>a\*</sup>, I. L. Ikhioya<sup>d</sup>,  
K. I. Udofia<sup>a</sup>, J. Effiom-Edem Ntibi<sup>b</sup>, C. N. Ozoemena<sup>e</sup>, and M. A. Abua<sup>f</sup>

<sup>a</sup>*Department of Physics and Industrial Physics, Faculty of Physical Sciences, Nnamdi Azikiwe University, Awka, Nigeria.*

*\*e-mail: agobi@unical.edu.ng*

<sup>b</sup>*Department of Physics, Faculty of Physical Sciences, University of Calabar, Calabar, Nigeria.*

<sup>c</sup>*Materials Chemistry Research Group, Department of Pure and Applied Chemistry,  
Faculty of Physical Sciences, University of Calabar, Calabar, Nigeria.*

<sup>d</sup>*Department of Physics and Astronomy, Faculty of Physical Sciences, University of Nigeria, Nsukka, Enugu State, Nigeria.*

<sup>e</sup>*Department of Radiography and Radiological sciences, Faculty of Allied Medicine, University of Calabar, Calabar, Nigeria.*

<sup>f</sup>*Department of Geography and Environmental Sciences, Faculty of Environmental Sciences,  
University of Calabar, Calabar, Nigeria.*

Received 31 March 2022; accepted 6 September 2022

Novel ternary nanocomposite films based on polyvinylpyrrolidone copper nanoparticles graphene oxide (PVP/Cu/GO) were prepared using electrochemical deposition technique on Fluorine doped tin oxide (FTO) substrate. This facile and effective approach has been proven to be very useful for the fabrication of inexpensive, high-performance electrochemical devices. To achieve uniform deposition of the nanocomposite films, the three components of the nanocomposites were mixed under controlled conditions. The impact of different GO loading on the PVP/Cu/GO composites was measured using ultraviolet-visible spectrophotometry (UV-vis), X-Ray Diffraction (XRD) spectroscopy, scanning electron microscopy (SEM), Energy dispersive X-ray spectroscopy (EDX), and four-point probe techniques to evaluate their optical, structural, morphological, compositional, and electrical properties, respectively. UV-visible analysis shows that the optical band gap ( $E_g$ ) of the nanocomposite decreased from 3.51 to 2.02 eV with increasing GO loading. All of the nanocomposites showed UV absorbance of  $\approx 450$  nm. According to the XRD results, the GO materials were very well dispersed in the PVP/Cu/GO composites, while also revealing the crystalline nature of the nanocomposites. The SEM results revealed spherical-shaped grains of the deposited films, while the EDX results revealed the major elements deposited. Four-point probe analysis of the nanocomposites revealed slight increase in conductivity with low GO content, thus confirming the semiconducting properties of the nanocomposites with the GO content. The obtained results herein shows that the PVP/Cu/GO nanocomposites are successfully synthesized with attractive physiochemical properties suitable for the fabrication of organic electronic devices and photovoltaic devices.

**Keywords:** Graphene oxide; polymer; polyvinylpyrrolidone; nanocomposites.

DOI: <https://doi.org/10.31349/RevMexFis.69.031001>

## 1. Introduction

Nanocomposite materials have been a major area of research interest owing to their distinct electrochemical properties that differ significantly from those of their constituent components [1]. Similarly, devices based on polymer nanocomposites have received an enormous attention owing to their ability to solve both energy and environmental problems. Polyvinylpyrrolidone (PVP) is one of the water-soluble low-cost polymers that possess non-ionic and nontoxic properties with pore-forming macromolecules, good film forming stability, and appealing chemical properties [2]. PVP is widely used in the design of materials for various applications. Nanocomposite technology based on nanofillers such as graphene derivatives like graphene oxide (GO), and reduced graphene oxide (rGO) has already been considered to be an effective method for producing novel materials with excellent properties and high performance [3]. Because of the presence of oxygen functional groups on its basal planes

and edges, GO is thought to be a functionalized graphene [4]. The functional groups in GO permit non-covalent and covalent chemical functionalization, which is particularly useful in the formation of nanocomposites [5]. Interestingly, GO has gotten a lot of attention because of its ability to function as a precursor to some conductive materials [6-8]. More specifically, because of the high compatibility of PVP and GO and their good miscibility in water, the growth of films from such components is expected to be of great interest [3]. Nonetheless, despite recent advances in polymer graphene oxide nanocomposites, incorporation of metals or metal oxides, carbon nanomaterials, and polymers into the polymer matrix has been sought to improve their properties because of synergistic effects [9,10]. These hybrid nanocomposites also help to minimize some of the drawbacks experienced in polymer based devices like low chemical stability and mechanical properties [11,12]. Because of its low cost, availability, potency, electrochemical properties, good anti-interference potential, and processability into nanosized material, copper is

an intriguing metal choice. Copper, in particular, has been used in solar cells and electronic materials, making it very appealing to researchers [13]. In this study, PVP polymer, copper nanoparticles and graphene oxide (GO) nanoparticles were incorporated together for the electrochemical deposition of ternary nanocomposite PVP/Cu/GO films. The current study sought to ascertain the effect of GO addition on the optical, morphology, and structural properties of PVP/Cu/GO nanocomposite films.

## 2. Experimental section

### 2.1. Chemicals and materials

In this study, we used analytical grade polyvinylpyrrolidone (PVP), copper sulfate pentahydrate ( $\text{CuSO}_4 \cdot 5\text{H}_2\text{O}$ ), graphite powder; sulphuric acid ( $\text{H}_2\text{SO}_4$ ), potassium permanganate ( $\text{KMnO}_4$ ) and fluorine doped tin oxide (FTO) substrate. These chemicals were used as received from commercial suppliers with no additional treatment, while deionized water (DIW) was utilized throughout the experiment.

### 2.2. Synthesis of PVP/Cu/GO nanocomposite

Graphene oxide (GO) was first synthesized from natural graphite using a modified Hummers procedure as described in the literature [14]. Then, 0.5 g/mol of synthesized GO nanoparticle was dissolved in 100 mL of DIW and stirred for 1 hour in a beaker with a magnetic stirrer to obtain a homogeneous GO aqueous solution, which was used to prepare PVP/Cu/GO nanocomposites. Following that, a 0.01 M PVP solution was made by dissolving 0.11 g/mole in 100 mL of DIW and stirring for 1 hour. Similarly, 1.25 g/mol  $\text{CuSO}_4 \cdot 5\text{H}_2\text{O}$  (0.01 M) solution was made by dissolving it in 500 mL of DIW. 15 mL of 0.01 M PVP and 10 mL of 0.01 M Cu were filled in a beaker and stirred for 2 hours to obtain homogeneous PVP and Cu dispersions. Finally, the already prepared GO aqueous solution was incorporated into the PVP and Cu solution and stirred for 2 h using a magnetic stirrer to obtain homogeneous PVP/Cu/GO solutions. The GO content was varied to 0.0, 0.4, 0.6 and 0.8 wt% in relation to the amount of PVP and Cu solution. An electrochemical deposition method was employed to form the nanocomposites while the PVP/Cu/GO solutions served as the electrolyte. fluorine doped tin oxide (FTO) substrate used for the deposition were cleaned and clipped in between two-electrode cell while a large-area platinum sheet acts as the counter electrode and a pseudo-reference electrode. The substrates were then immersed in the electrolyte for 60 seconds at a constant voltage of 15 volts in an electrochemical setup. The current and potential drop passing through the films were assessed with the aid of a sensitive ammeter and a voltmeter. Finally, composite-coated glasses were obtained and washed with deionized water after electrodeposition to remove any unreacted substances before being dried at room temperature.

### 2.3. Characterizations

Some spectroscopic methods were used in analyzing the optical, structural, morphological and compositional properties of the synthesized nanocomposite films. They include; UV-1800 visible spectrophotometer in the wavelength range of 300-1100 nm, Bruker D8 Advance XRD with a Cu K line ( $\lambda = 1.54056 \text{ \AA}$ ) in  $2\theta$  ranges from  $10^\circ$  to  $90^\circ$ , SEM, EDX, while the electrical properties of the nanocomposite films were studied using the Jandel four-point probes technique (model T345).

## 3. Results and discussion

### 3.1. Optical properties of PVP/Cu/GO nanocomposites

The interaction of photon energy with the surface of a material results to absorption, transmission and reflection [15,16]. These three properties are related by Eq. (1). However, the understanding of transmittance aids in determining the energy band gap and band structure of materials.

$$A + T + R = 1, \quad (1)$$

where  $A$  absorbance,  $T$  transmittance, and  $R$  reflectance.

Absorbance however is the negative logarithm to base 10 of the transmittance,

$$A = -\log_{10} \frac{I_t}{I_0} = -\log_{10} T. \quad (2)$$

It follows from Eq. (2) that the transmittance and absorbance are related by

$$T = 10^{-A}. \quad (3)$$

Figure 1a) illustrates the dependence of the absorbance on the wavelength of the PVP/Cu/GO films in the range 300-1100 nm. According to the diagram, all of the films have nearly the same absorbance spectral, with the highest absorbance in the UV region of  $\approx 450 \text{ nm}$ , but decreased significantly as they moved into the NIR region of the spectrum. This behavior is attributed to the possible interactions that exist between the GO and long aromatic rings of the polymer chain [17], which could be responsible for the improvement of light absorption of the films in the UV-Vis region, thereby enhancing some photovoltaic properties such as photocatalytic efficiency and photoluminescence of the films. However, as the GO loading increases, the absorption remains relatively constant. The transmittance  $T$  versus wavelength plots as calculated from Eq. (3) indicates that the PVP/Cu/0.0% shows transmittance of  $\approx 30\%$  which increased with increasing GO loading from (0.4% to 0.8%) to about 70% as revealed in Fig. 1b). Nonetheless, all the films have low transmittance ( $\approx 400 \text{ nm}$ ) in the UV region of the electromagnetic spectrum, which increases with increasing wavelength up to the NIR region. The low transmissions of the films reflect the change observed in the optical band gap,

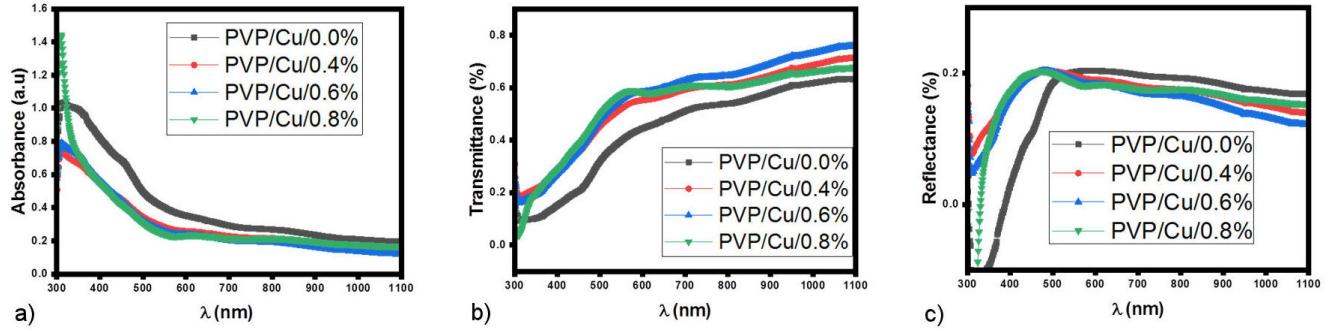


FIGURE 1. a) absorption spectra versus wavelength, b) transmittance versus wavelength, and c) reflectance versus wavelength plots of PVP/Cu/GO nanocomposites with varying GO loadings.

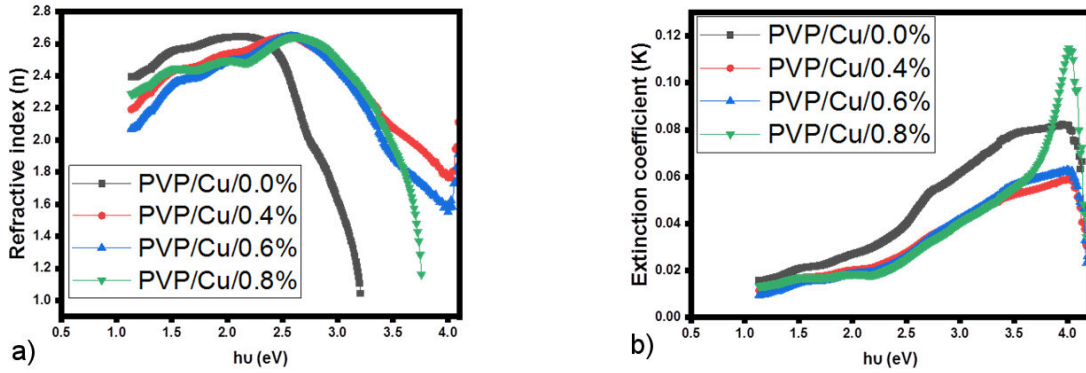


FIGURE 2. a) Refractive Index versus  $h\nu$  and b) Extinction Coefficient versus  $h\nu$  plots of PVP/Cu/GO nanocomposites with varying GO loading.

which was a consequence of the change in the band structure of PVP matrix. The films' low transmittance makes them useful in solar thermal energy collectors and active layers for solar cell applications [18], thus, these absorbance and transmittance results suggest the potential application of the nanocomposite in energy-related devices. Figure 1c) shows that the films' reflectance  $R$  is generally low across the electromagnetic spectrum; an all-out of 20% in the UV region.

The refractive index  $n$  is the ratio of radiation speed between two media; this property aids in the evaluation of a material for use in anti-reflective coatings for solar cells. It is related with the optical reflectance according to Eq. (4) [19,20].

$$n = \frac{([R^{1/2}] - 1)}{([R^{1/2}] + 1)}, \quad (4)$$

where  $n$  refractive index and  $R$  reflectance,

$$K = \frac{\alpha\lambda}{4\pi}, \quad (5)$$

where  $\alpha$  absorption coefficient and  $\lambda$  wavelength.

The variation of the refractive index of the films with the photon energy as shown in Fig. 2a), exhibits a non-linear feature which indicates a departure from the films normal dispersion behavior hence, for all films, high values of refractive index are observed which indicates that the films deposited are of high density which consequently lower the inter-atomic spacing as was observed from the XRD results [21]. Owing to the high values of the refractive index of the deposited

films, they can be utilized in the design of optical waveguides [22]. The extinction coefficient  $K$  from Eq. (5) estimates the level of light lost when scattering and absorption occurs [23], hence, Fig. 2b) reveals that an increase in photon energy causes an increase in the extinction coefficient values all the films for the different GO loadings, with the PVP/Cu/0.0% film having the least extinction coefficient. This behavior revealed the films as having high extinction coefficient values in the UV-region and low values in the infrared region, thus exhibiting an intriguing property typical of photonic materials [24]. The extinction coefficients of the samples range from 1.01 to 4.01 eV.

To get an insight about the optical shift which occurs when a valence electron migrates to the conduction band of a material, we explore the correlation between the absorption coefficient  $\alpha$  and the photon energy  $h\nu$  [24,25]. When a photon of known energy in transmitted radiation is absorbed, an electron moves from the material's valence to conduction band. Changes in transmitted radiation provide information about the types of electron transitions that may occur. The excited - state transition is known as fundamental or basic absorption, and it is characterized by a rapid increase in absorption known as the absorption edge, which is used to calculate the optical band gap from [27] Eq. (6).

$$\alpha h\nu = B(h\nu - E_g)^{1/2}, \quad (6)$$

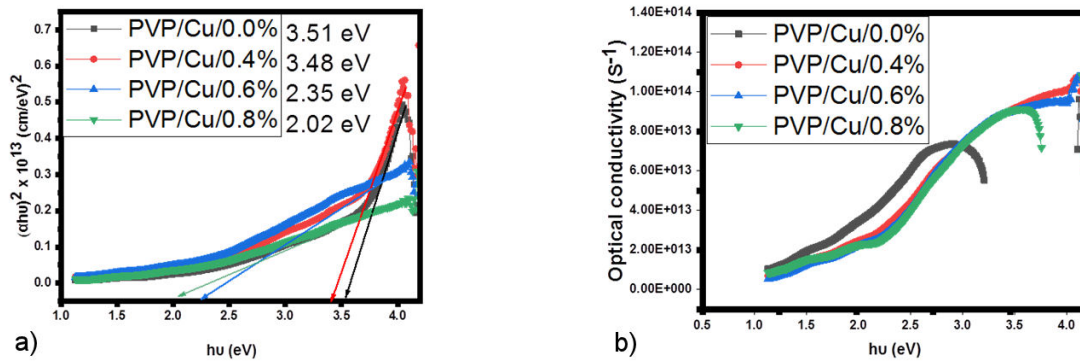


FIGURE 3. a)  $(\alpha h\nu)^2$  versus  $h\nu$  b) optical conductivity versus  $h\nu$  plots of PVP/Cu/GO nanocomposites with varying GO loading.

where  $E_g$  band gap energy,  $\alpha$  absorption coefficient,  $B$  constant which is dependent on the sample structure,  $\nu$  frequency of the incident light and  $h$  Planck's constant.

For direct band gap materials, Eq. (6) determines the absorption coefficient and photon energy [26]. However, the absorption coefficient, the absorbance and the films' thickness  $d$  are related by Eq. (7).

$$\alpha = 2.303 \frac{A}{d}, \quad (7)$$

where  $\alpha$  absorption coefficient,  $A$  absorbance and  $d$  films thickness.

Nonetheless, the optical band gap of pure PVP has been reported elsewhere as 3.88 eV [28].

Hence, in the present study, the optical band gap of PVP/Cu/0.0% nanocomposites before incorporation of GO was found to be 3.51 eV, as shown in Fig. 3a). This reduction in optical band gap of the PVP/Cu/0.0% can be attributed to the presence of chemical bonding that exists between the PVP long aromatic rings and Cu nanoparticles. This behavior shows that Cu nanoparticles will influence more localized energy states which will control the optical and electrical characteristics and hence modify the band structure of PVP matrix. However, upon interaction with GO at various loadings (0.4% to 0.8%), the direct band gap narrowed to a value of 3.51 to 2.02 eV. This result indicates that the introduction of the GO further resulted to addition of energy levels inside the band structure of the films, and consequently reduced the optical band gap. Thus, by simply changing the GO content, the optical band gap of the nanocomposites can be controlled. The optical band gap ( $E_g$ ) values of the films are obtained by extrapolating the linear region of the  $(\alpha h\nu)^2$  against  $h\nu$  plot to intercept the photon energy axis, that is, taking the best fit of the curve  $(\alpha h\nu)^2 = 0$  as revealed in Fig. 3a). In a similar way, the optical feedback of a transparent materials is refers to as its optical conductivity ( $\sigma$ ) given in Eq. (8) [29,30].

$$\sigma = \frac{\alpha n c}{4\pi}. \quad (8)$$

Figure 3b) shows an increasing trend for the optical conductivity of all the films by an increasing photon energy, resulting in an increase in the films' conductivity which suggests that they have good photo-response and could be used

as photoconductors [31]. All the films show the same trend within the UV region of the spectrum where the films exhibit optimum optical conductivity. These types of materials are thought to be favorable for various optoelectronic device applications [32].

A material's dielectric constant  $\varepsilon$  is a parameter that is used to estimate the degree to which the speed of light is shaded off throughout the material and how much energy is absorbed by a dielectric material due to dipole movement in an electric field [33]. It is shown in Eq. (9). Hence, it turns out that the dielectric constant is of two parts namely; the real  $\varepsilon_r$  and imaginary  $\varepsilon_i$  parts as shown in Eq. (9-12) [34].

$$\varepsilon = (n + iK)^2, \quad (9)$$

$$\varepsilon = \varepsilon_r + \varepsilon_i, \quad (10)$$

$$\varepsilon = n^2 - K^2, \quad (11)$$

$$\varepsilon = 2nK, \quad (12)$$

where  $n$  refractive index,  $K$  extinction coefficient,  $\varepsilon_r$  real part that represents the degree of polarization, as the degree of polarization increases, so does  $\varepsilon_r$ .  $\varepsilon_i$  imaginary part which represent dielectric losses.

The dielectric constant is also frequency dependent; in other words, frequency affects the value of the dielectric constant because the polarization mechanisms are unable to keep up with the rapidly changing field, and increasing frequency decreases the value. Plots of the real (RDC) and imaginary (IDC) dielectric constants versus photon energy of the PVP/Cu/GO nanocomposite films are shown in Figs. 4a) and 4b). From the plots, it is evident that the real dielectric possesses much higher values than the imaginary dielectric as all the films show similar pattern in RDC while increasing with a rise in photon energy to a value above 2.2 eV and drastically experiences a drop at higher photon energy values. Meanwhile, the imaginary dielectric from Fig. 4a) exhibits a near linear relationship with photon energy, increasing with increasing photon energy above 2.7 eV for all films. In general, this characteristic suggests a switching capability of the deposited PVP/Cu/GO film materials, and also shows that PVP/Cu/GO nanocomposites can serve as photovoltaic devices.

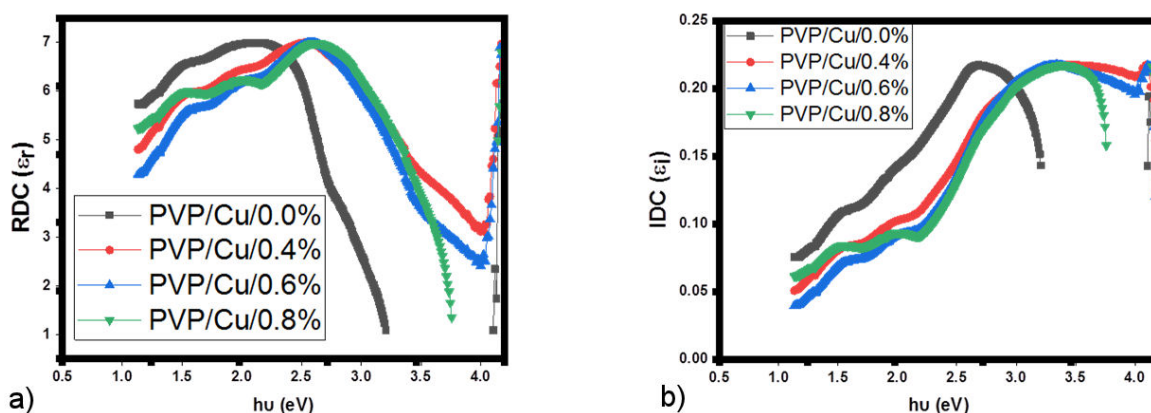


FIGURE 4. a) Real dielectric constant b) Imaginary dielectric constant versus  $h\nu$  plots of PVP/Cu/GO nanocomposites with varying GO loading.

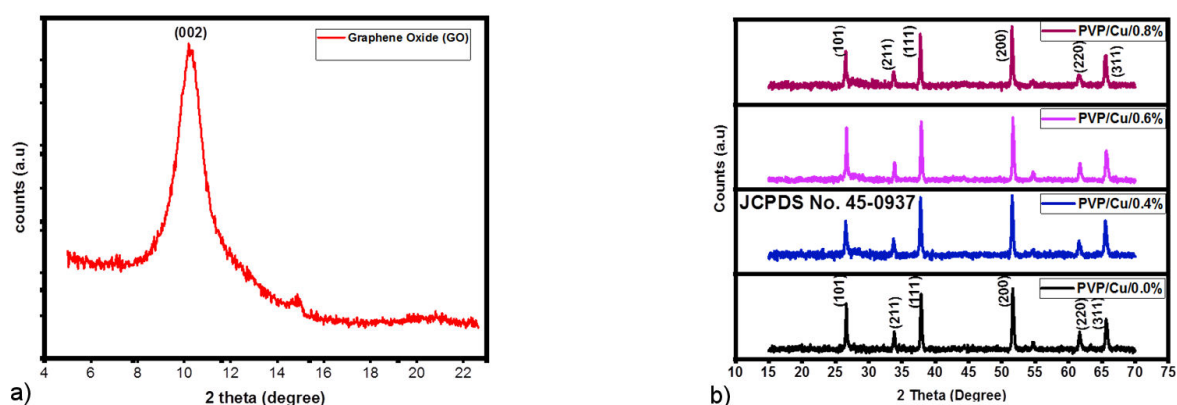


FIGURE 5. XRD pattern of PVP/Cu/GO films deposited at different GO loading.

### 3.2. X-ray diffraction

X-ray diffraction (XRD) measurements were used to examine the structure of the PVP/Cu/GO ternary nanocomposite films and the synthesized GO. The X-ray diffraction pattern was produced at a ( $\lambda = 1.54056$ ) in the 2 theta degree range from 100 – 900. Figure 5a) depicts the XRD of the synthesized GO which shows a strong peak at  $2\theta = 10.21$ , corresponding to the miller index (002) reflection peak. As reported in the literature [35], GO has its highest intensity peak at 2 theta between 10-120; thus, the X-ray diffraction pattern confirmed the successful formation of GO. Figure 5b) depicts the XRD curves of the various PVP/Cu/GO films. The plots show that all of the films' characteristic peaks occurred at the same reflection angles. Only typical CuO peaks are visible at  $2\theta = 27.10, 34.50, 38.20, 52.30, 62.20$  and  $67.40$ , which are indexed at (101), (211), (111), (200), (220), and (311), all of which belong to the monoclinic phase of CuO in the JCPDS No 45-0937. These findings suggest that during the film formation process, the Cu nanoparticles may have interacted with the oxygen in the reacting environment, resulting in copper oxidation and the formation of CuO [22]. The lack of a GO diffraction peak in the XRD pattern indicates that the GO sheets are uniformly distributed in the nanocomposites with negligible aggregation [36]. The ob-

served sharp peaks indicate that the synthesized films have good crystallinity [37]. The size of the crystallinity was calculated using Scherrer's equation [38-42].

$$D = \frac{0.94\lambda}{\beta \cos \theta}, \quad (13)$$

where  $\beta$  is the full width at half maximum (FWHM) of the most strong diffraction peak, and  $\lambda$  wavelength of incident radiation (1.54056). The synthesized nanocomposite has a crystallinity size of 7 nm.

### 3.3. Morphology study

Using scanning electron microscopy images, surface morphological studies of various PVP/Cu/GO films with varying GO loading were investigated (SEM). Figure 6 compares the morphological characteristics of films. Figure 6a) shows that the PVP/Cu/0.0% nanocomposite had spherical shapes and homogeneous particle distributions due to the compatibility interface between the PVP matrix and the Cu nanoparticles. However, as shown in Figs. 6b)-d), the surface morphology of the PVP/Cu/GO nanocomposites has changed significantly after the addition of GO at various loadings (0.4%, 0.6%, and 0.8%), resulting in relatively large nano fine-grained grains;

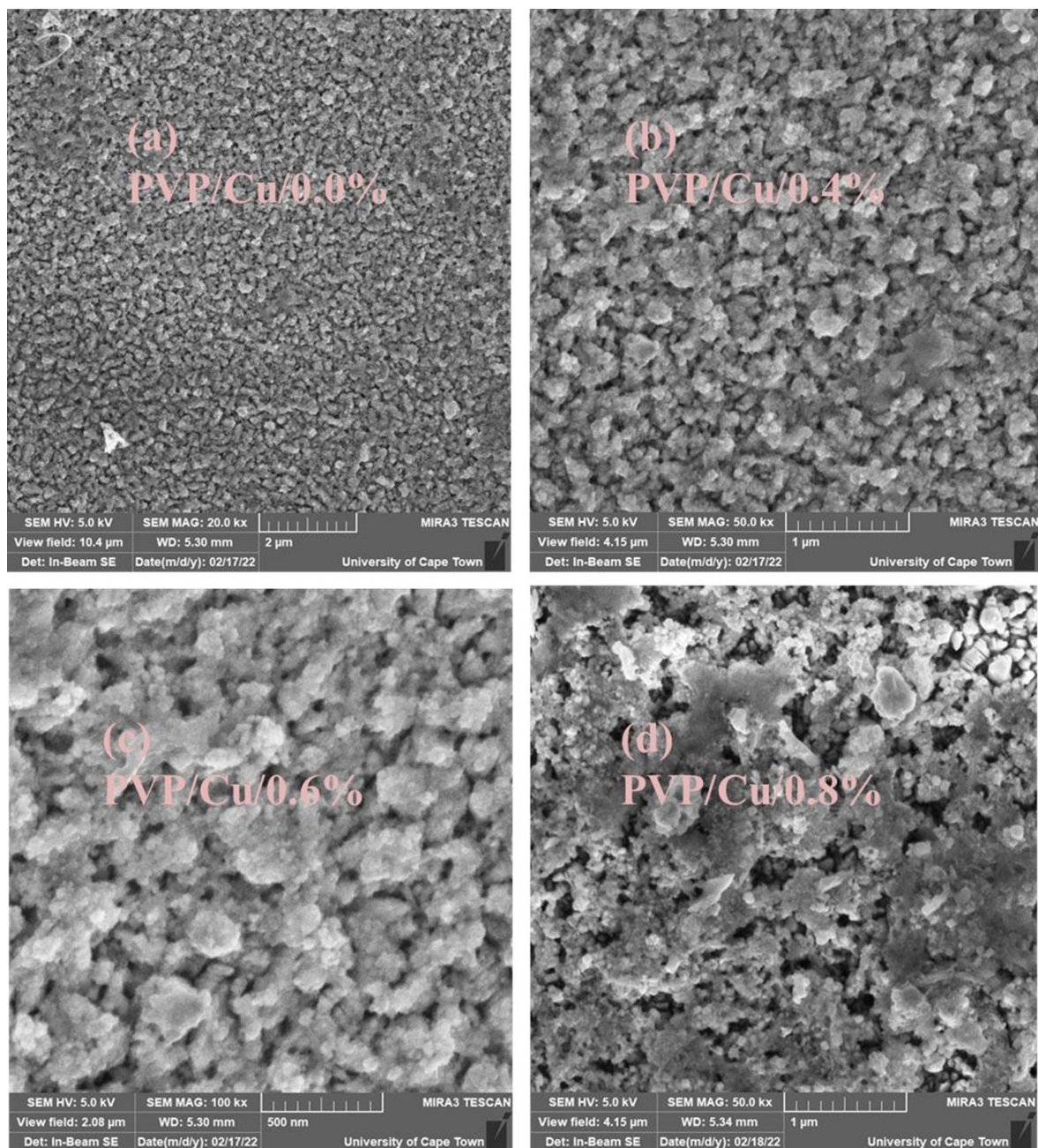


FIGURE 6. SEM Images of PVP/Cu/GO nanocomposites.

this behavior can confirm the required conductivity for the nanocomposite films [43].

### 3.4. EDX analysis

Figure 7 is a representative spectrum of the ternary PVP/Cu/GO nanocomposite with a graphene oxide load of 0.8%, similar spectra were obtained at other graphene oxide loads. The figure depicts the elemental compositions of the PVP/Cu/GO nanocomposite films. The graph clearly shows that the films contain the expected elements of carbon, nitrogen, copper, and oxygen as the main constituents of the

deposited films. The EDX result validates the synthesis of a new PVP/Cu/GO nanocomposite.

### 3.5. Electrical properties of PVP/Cu/GO nanocomposite

The electrical conductivity level of the PVP/Cu/GO nanocomposite films was estimated using a four-point probe system. The particles nanostructure of a nanocomposite film plays an important role in determining its electrical characteristics [44-46]. To ensure good ohmic contact with the films, the voltage across the transverse distance of the films and the corresponding current values were measured using silver

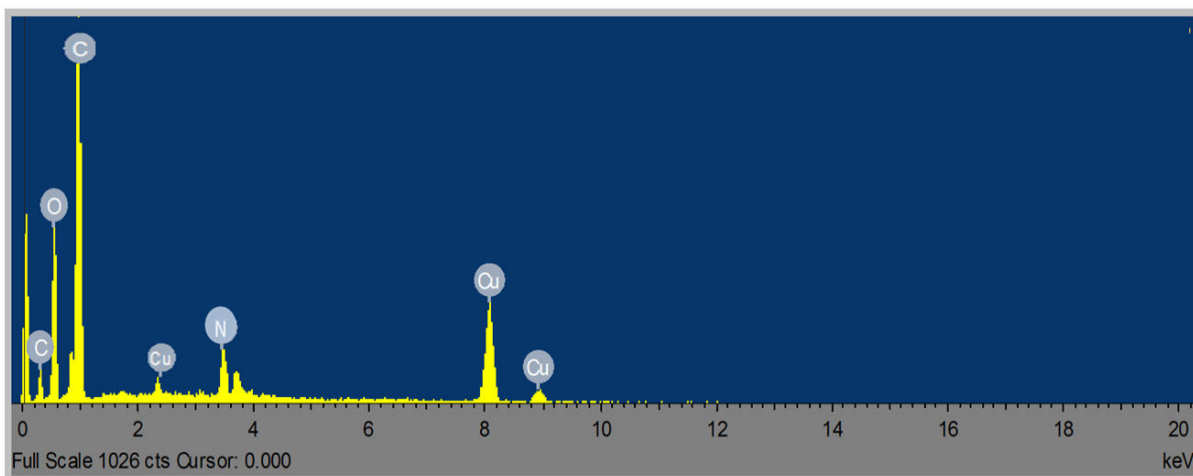


FIGURE 7. EDX spectrums of PVP/Cu/GO nanocomposites loaded with 0.8% GO.

TABLE I. Electrical measurements of PVP/Cu/GO nanocomposite

Samples	Thickness $t$ (nm)	Conductivity $\sigma(\Omega\text{m/cm})^{-1}$	Resistivity $\rho(\Omega\text{cm})$
PVP/Cu/0.0%	102.02	$8.711 \times 10^{-8}$	$1.147 \times 10^{-9}$
PVP/Cu/0.4%	104.02	$8.729 \times 10^{-8}$	$1.145 \times 10^{-9}$
PVP/Cu/0.6%	105.01	$8.734 \times 10^{-8}$	$1.144 \times 10^{-9}$
PVP/Cu/0.8%	105.02	$8.752 \times 10^{-8}$	$1.142 \times 10^{-9}$

paste in a typical setup. The resistance values of the deposited films were investigated. The four point probes were linked to a current supply, while the inner probes were linked to a voltmeter. The voltage drop across the probes is measured as current flows between the outer probes. The thickness, resistivity, and conductivity values of PVP/GO/Cu films are summarized in Table I. The results show that the material deposited with different GO loading increases in thickness from 102.02 to 105.02 nm with a corresponding decrease in resistivity from  $1.147 \times 10^{-9}$  to  $1.142 \times 10^{-9}$   $\Omega\text{m}$ , consequently increasing electrical conductivity of the films. The slight increase in conductivity could be attributed to stacking of the GO layers in the nanocomposites, which improves electron mobility within the nanocomposite system. According to [17], GO, having a large surface area, has the potential to be an effective percolative conducting bridge, thus increasing the conductivity of the nanocomposite.

#### 4. Conclusions

The electrochemical deposition method was successfully utilized for the synthesis of polymer, copper, graphene oxide nanocomposites (PVP/Cu/GO) with different GO loading. Various complementary techniques; UV-Vis, XRD, SEM, EDX, and a four-point probe were used to investigate the effect of GO loading on the optical, structural, morphological, compositional, and electrical properties of the different films

for applications in photovoltaic devices. It was observed that the GO loading reduced the optical band gap of the nanocomposites from 3.51 to 2.02 eV. The optical results also showed highest absorbance in the UV region  $\approx 450$  nm. The XRD pattern reveals that the deposited films were crystalline in nature, exhibiting major reflection peaks at (101), (211), (111), (200), (220) and (311) lattice planes. With increase in GO loading, the SEM micrograph showed relatively large nano fine-grained grains indicating uniform deposition. The presence of carbon, nitrogen, copper, and oxygen as major elemental constituents of the films was confirmed by the EDX results. The four point probe results revealed that the GO content improved the nanocomposite's conductivity thereby confirming the semiconducting nature of the films. Owing to these results, the PVP/Cu/GO nanocomposite has great potential in photovoltaic applications.

#### Acknowledgments

Augustine U. Agobi is very much thankful to the Petroleum Technology Development Fund (PTDF).

#### Author contribution statement

Augustine U. Agobi: Conceptualization, Formal analysis, Investigation, Writing - review & editing. Alexander I. Ikeuba: Validation, Resources, Writing - review & editing. Azubike J. Ekpunobi: Supervision, Conceptualization, Project administration. Imosobomeh L. Ikhioya: methodology & graphical plots. Udofia, Kuffre Imoh: Analysis, Writing - review & editing. Joseph Effiom-Edem Ntibi: Analysis, Writing - review & editing. Chiaghanam N. Ozoemena: proofreading, initial corrections, & suggestions. Abua Moses Adah: Analysis, proofreading, & editing.

#### Conflict of interest

The authors declare no conflict of interest.

1. L. Cao, Y. Liu, and B. Zhang, In situ controllable growth of Prussian blue nanocubes on reduced graphene oxide: facile synthesis and their application as enhanced nanoelectrocatalyst for H<sub>2</sub>O<sub>2</sub> reduction, *ACS Appl Mater Interfaces* **2** (2010) 2339.
2. S.J. Guo, S.J. Dong, and E. Wang, Three-dimensional Pt-on-Pd bimetallic nanodendrites supported on graphene nanosheet: facile synthesis and used as an advanced nanoelectrocatalyst for methanol oxidation, *ACS Nano* **4** (2010) 547.
3. M. El Achaby *et al.*, Graphene oxide reinforced chitosan/polyvinylpyrrolidone polymer bio-nanocomposites, *Journal of Applied Polymer Science* **131** (2014).
4. Y. Sun, Q. Wu, and G. Shi, Graphene based new energy materials, *Energy Environ. Sci.* **4** (2011) 1113.
5. M. Masoumparast, M. Mokhtary, and H. Kefayati, Preparation and characterization of polyvinylpyrrolidone/cobalt ferrite functionalized chitosan graphene oxide (CoFe<sub>2</sub>O<sub>4</sub>@CS@GO-PVP) nanocomposite, *Journal of Polymer Engineering* **4** (2020) 342.
6. M. Savchak *et al.*, Highly conductive and transparent reduced graphene oxide nanoscale films via thermal conversion of polymer-encapsulated graphene oxide sheets, *ACS Appl. Mater. Interfaces* **104** (2018) 3975.
7. L. He, S.C. Tjong, Facile synthesis of silver-decorated reduced graphene oxide as a hybrid filler material for electrically conductive polymer composites, *RSC Adv* **3** (2013) 22981.
8. K.S.U. Schirmer, D. Esrafilzadeh, B.C. Thompson, A.F. Quigley, R.M.I. Kapsa, and G.G. Wallace, Conductive composite fibres from reduced graphene oxide and polypyrrole nanoparticles, *J. Mater. Chem. B* **4** (2016) 1142.
9. R. Megha *et al.*, AC conductivity studies in copper decorated and zinc oxide embedded polypyrrole composite nanorods: *Interfacial effects*, *Materials Science in Semiconductor Processing*, (2020).
10. R. Ullah, S. Bilal, A. Ali Shah, G. Rahman, and K. Ali, Ternary composites of polyaniline with polyvinyl alcohol and Cu by inverse emulsion polymerization: a comparative study, *Adv. Polym. Technol.* **37** (2018) 3448.
11. A.T. Mane, S.T. Navale, R.C. Pawar, C.S. Lee and V.B. Patil, Microstructural, optical and electrical transport properties of WO<sub>3</sub> nanoparticles coated polypyrrole hybrid nanocomposites, *Synth. Met.* **199** (2015) 187.
12. E. Ozkazanc, Polypyrrole/copper(II) acetylacetonate composites prepared by in situ chemical oxidative polymerization, *Synth. Met.* **162** (2012) 1016.
13. Y. Ma *et al.*, A novel core-shell polyaniline/graphene oxide/copper nanocomposite for high performance and low-cost supercapacitors, *Chemical Papers* (2018).
14. Y. Liu, Q. Li, and Y.Y. Feng, Immobilisation of acid pectinase on graphene oxide nanosheets *Chem Pap.* **68** (2014) 732.
15. P. Nwofe, Influence of film thickness on the optical properties of antimony sulphide thin film grown by the solution growth technique, *European Journal of Applied Engineering and Scientific Research* **4** (2015) 1.
16. O. Abdullah, S. Ghareb, and R. Dlear, Optical Absorption of Polyvinyl Alcohol Films Doped with Nickel Chloride. *Applied Mechanics and Materials* **5** (2011) 110.
17. C. Bora, and S.K. Dolui, Fabrication of polypyrrole/graphene oxide nanocomposites by liquid/liquid interfacial polymerization and evaluation of their optical, electrical and electrochemical properties, *Polymer* **53** (2012) 923.
18. J.I. Onwuemeka, and A.J. Ekpunobi, Synthesis of CdO:SnO<sub>2</sub> alloyed thin films for solar energy conversion and optoelectronic applications, *J. Mater. Sci. Mater. Electron.* **29** (2018) 9176.
19. M. Banerjee, A. Jain, and G.S. Mukherjee, Microstructural and optical properties of polyvinyl alcohol/manganese chloride composite film, *Polymer Composites*, (2018).
20. A.H. Majeed, H. Hussein, and H. Ahmed, Studying the Optical Properties of (PVA-PEG-KBr) Composite, *International Journal of Science and Research* **3** (2014).
21. M. Abdelaziz, Cerium (III) doping effects on optical and thermal properties of PVA films *Physica B* **406** (2011) 1300.
22. R. Jyoti, S. Isha, S. Annu, C. Navneet, A. Sanjeev, D. Rajnish, and K. S. Pawan, Cu nanoparticles induced structural, optical and electrical modification in PVA, *Materials Chemistry and Physics* **134** (2012) 1121.
23. S. Gedi, V.R.M. Reddy, C. Park, and J. Chan-Wook, Comprehensive optical studies on SnS layers synthesized by chemical bath deposition, *Opt. Mater.* **42** (2015) 468.
24. I.L. Ikhioya, A.C. Nkele, S. N. Ezema, M. Maaza, and F. Ezema, A study on the effects of varying concentrations on the properties of ytterbium-doped cobalt selenide thin films, *Optical Materials*, (2020).
25. S. Gedi, V.R.M. Reddy, C. Park, and J. Chan-Wook, Comprehensive optical studies on SnS layers synthesized by chemical bath deposition, *Opt. Mater.* **42** (2015) 468.
26. T.S. Soliman, and A.S. Abouhaswa, Synthesis and structural of Cd<sub>0.5</sub>Zn<sub>0.5</sub>F<sub>2</sub>O<sub>4</sub> nanoparticles and its influence on the structure and optical properties of polyvinyl alcohol films, *Journal of Materials Science: Materials in Electronics*, (2020).
27. N. Baraz, I. Yücedağ, Y. Azizian-Kalendaragh, and S. Altindal Determining electrical and dielectric parameters of dependence as function of frequencies in Al/ZnS-PVA/p-Si(MPS) structures. *J Mater Sci Mater Electron* **28** (2017) 1315.
28. K. Sreekanth, T. Siddaiah, N.O. Gopal, K.Y. Madhava and C. Ramu, Optical and electrical conductivity studies of VO<sub>2</sub>+doped polyvinyl pyrrolidone (PVP) polymer electrolytes. *Journal of Science, Advanced Materials and Devices*, (2019).
29. S.U. Offiah, P.E. Ugwoke, A.B.C. Ekwealor, S.C. Ezugwu, R.U. Osuji, and F.I. Ezema, Structural and spectral analysis of chemical bath deposited copper sulfide thin films for solar energy conversions, *Digest Journal of Nanomaterials and Biostructures* **7** (2012) 165.
30. A.U. Agobi, A.J. Ekpunobi, A. I. Ikeuba, and H. Louis, the effects of graphene oxide load on the optical, structural and electrical properties of ternary nanocomposites (Polyvinyl alcohol/copper/graphene oxide) for electronic and photovoltaic application. *Results in Optics* **8** (2022) 100261.

31. K.T. Al-Rasoul, N.K. Abbas, and Z. J. Shanan, Structural and optical characterization of Cu and Ni doped ZnS nanoparticles, *Int. J. Electrochem. Sci.* **8** (2013) 594.
32. P. C. Okafor, A. J. Ekpunobi, and P.A Ekwo, Effect of manganese percentage doping on thickness and conductivity of zinc sulphide nanofilms prepared by electrodeposition method, *International Journal of Science and Research (IJSR)* **4** (2014) 5.
33. H. Ahmed, and H. Noor, UV-Absorption for Biological Application of (Polymer- Carbide) Nanocomposites, *Research Journal of Agriculture and Biological Sciences* **13** (2018).
34. T.S Soliman, and S.A Vshivkov, Effect of Fe nanoparticles on the structure and optical properties of polyvinyl alcohol nanocomposite films, *Journal of Non-Crystalline Solids*, **519** (2019) 119452.
35. M. Li, X. Huang, C. Wu, H. Xu, P. Jiang, and T. Tanaka, Fabrication of two dimensional hybrid sheets by decorating insulating PANI on reduced graphene oxide for polymer nanocomposites with low dielectric loss and high dielectric constant, *J. Mater. Chem.* **22** (2012) 23477.
36. I.A.B Moura, T.G Sousa, A.M Lima, W.S Oliveira, and L.P Brandao, Synthesis and Characterization of Graphene-Oxide Reinforced Copper Matrix Composite, *Mater. Proc.* **4** (2021) 72.
37. A S Hassanien, and A. A Akl, Optical characterizations and refractive index dispersion parameters of annealed TiO<sub>2</sub> thin films synthesized by RF-sputtering technique at different flow rates of the reactive oxygen gas, *Physica B* **576** (2020) 411718.
38. A.C. Nkele, A study on titanium dioxide nanoparticles synthesized from titanium isopropoxide under SILAR-induced gel method: transition from anatase to rutile structure, *Inorg. Chem. Commun.* **112** (2020) 107705.
39. A.C. Nwanya, Nanoporous copper-cobalt mixed oxide nanorod bundles as high performance pseudocapacitive electrodes, *J. Electroanal. Chem.* **787** (2017) 24.
40. A.C. Nkele, Investigating the properties of nano nest-like nickel oxide and the NiO/Perovskite for potential application as a hole transport material, *Adv. Nat. Sci. Nanosci. Nanotechnol.* **10** (2019) 045009.
41. S.U. Offiah, Influence of cadmium precursor concentrations on the structural, optical and electrochemical impedance properties of CdZnS thin films, *Vacuum* **160** (2019) 246.
42. M.C. Nwankwo, Electrochemical supercapacitive properties of SILAR-Deposited Mn<sub>3</sub>O<sub>4</sub> electrodes, *Vacuum* **158** (2018) 206.
43. Y. Li, M. Jiao, H. Zhao, and M. Yang, High performance gas sensors based on in-situ fabricated ZnO/polyaniline nanocomposite: the effect of morphology on the sensing properties, *Sensor, Actuator. B Chem.* **264** (2018) 285.
44. A.U. Agobi, A.J. Ekpunobi, A.I. Ikeuba, I.L. Ikhioya, C.N. Ozoemena and K.I. Udofia, Hybrid polypyrrole/copper/graphene oxide nanocomposite films synthesized via potentiostatic deposition with enhanced photovoltaic properties. *Journal of the Indian Chemical Society*, **99** (2022) 100549.
45. B.I. Ita and A.I. Ikeuba, Solutions of the Dirac equation with gravitational plus exponential potential. *Applied Mathematics* **4** (2022) 1.
46. A.I. Ikeuba, B. Zhang, J. wang, E. H. Han, and W. Ke, Electrochemical, TOF-SIMS and XPS studies on the corrosion behavior of Q-phase in NaCl solutions as a function of pH. *Applied Surface Science*, **490** (2022) 535.